Discrete solution of the electrokinetic equations

Capuani, F.; Pagonabarraga, I.; Frenkel, D.

DOI
10.1063/1.1760739
Publication date
2004

Published in
Journal of Chemical Physics

Discrete solution of the electrokinetic equations

Fabrizio Capuani[a)]
FOM Institute for Atomic and Molecular Physics (AMOLF), Kruislaan 407, 1098 SJ Amsterdam, The Netherlands

Ignacio Pagonabarraga[b)]
Departament de Física Fonamental, C. Martí i Franqués 1, 08028 Barcelona, Spain

Daan Frenkel
FOM Institute for Atomic and Molecular Physics (AMOLF), Kruislaan 407, 1098 SJ Amsterdam, The Netherlands

(Received 2 March 2004; accepted 21 April 2004)

We present a robust scheme for solving the electrokinetic equations. This goal is achieved by combining the lattice-Boltzmann method with a discrete solution of the convection-diffusion equation for the different charged and neutral species that compose the fluid. The method is based on identifying the elementary fluxes between nodes, which ensures the absence of spurious fluxes in equilibrium. We show how the model is suitable to study electro-osmotic flows. As an illustration, we show that, by introducing appropriate dynamic rules in the presence of solid interfaces, we can compute the sedimentation velocity (and hence the sedimentation potential) of a charged sphere. Our approach does not assume linearization of the Poisson–Boltzmann equation and allows us for a wide variation of the Peclet number. © *2004 American Institute of Physics.*
[DOI: 10.1063/1.1760739]

I. INTRODUCTION

The study of the dynamics of suspensions of charged particles is interesting both because of the subtle physics underlying many electrokinetic phenomena and because of the practical relevance of such phenomena for the behavior of many synthetic and biological complex fluids.[1,2] In particular, electrokinetic effects can be used to control the transport of charged and uncharged molecules and colloids, using electrophoresis, electro-osmosis, and related phenomena.[3] As micro-fluidic devices become ever more prevalent, there are an increasing number of applications of electro-viscous phenomena that can be exploited to selectively transport material in devices with mesoscopic dimensions.[4]

In virtually all cases of practical interest, electroviscous phenomena occur in confined systems of a rather complex geometry. This makes it virtually hopeless to apply purely analytical modeling techniques. But also from a molecular-simulation point of view electroviscous effects present a formidable challenge. First of all, the systems under consideration always contain at least three components; namely a solvent plus two (oppositely charged) species. Then, there is the problem that the physical properties of the systems of interest are determined by a number of potentially different length scales (the ionic radius, the Bjerrum length, the Debye–Hückel screening length and the characteristic size of the channels in which transport takes place). As a result, fully atomistic modeling techniques become prohibitively expensive for all but the simplest problems. Conversely, standard discretizations of the macroscopic transport equations are ill-suited to deal with the statistical mechanics of charge distributions in ionic liquids, even apart from the fact that such techniques are often ill-equipped to deal with complex boundary conditions.

In this context, the application of mesoscopic (''coarse-grained'') models to the study of electrokinetic phenomena in complex fluids seem to offer a powerful alternative approach. Such models can be formulated either by introducing effective forces with dissipative and random components, as in the case of dissipative particle dynamics (DPD),[5] or by starting from simplified kinetic equations, as is the case with the lattice-Boltzmann method (LB).

The problem with the DPD approach is that it necessarily introduces an additional length scale (the effective size of the charged particles). This size should be much smaller than the Debye screening length, because otherwise real charge-ordering effects are obscured by spurious structural correlations; hence, a proper separation of length scales may be difficult to achieve. A lattice-Boltzmann model for electroviscous effect was proposed by Warren.[6] In this model, the densities of the (charged) solutes are treated as passive scalar fields. Forces on the fluid element are mediated by these scalar fields. A different approach was followed in Ref. 7, where solvent and solutes are treated on the same footing (namely as separate species). This method was then extended to couple the dynamics of charged colloids to that of the electrolyte solution. As we shall discuss below, both approaches have practical drawbacks that relate to the mixing of discrete and continuum descriptions.

The LB model that we introduce below appears at first sight rather similar to the model proposed by Warren. However, the underlying philosophy is rather different. We pro-

a)Electronic mail: capuani@amolf.nl, frenkel@amolf.nl
b)Electronic mail: ipagonabrraga@ub.edu

pose to consider the *fluxes* between connected nodes as the basic physical quantities that determine the evolution of local densities. Such a formulation ensures local mass conservation, does not rely on fluxes or gradients computed at the lattice nodes (which constitutes a source of error in other models due to the need to approximate them on a lattice), and by choosing a symmetric formulation for the link fluxes in terms of the nodes that are affected, we can recover the proper equilibrium without spurious fluxes. Our model relies on a LB formulation for mixtures. Hence, the improvements of the formulation based on link fluxes will overcome some of the limitation of previous LB models for mixtures based on gradient expansions of a free energy.[8]

The method described is very flexible, and, in particular, general boundary conditions are easily implemented. This feature also makes the proposed formulation attractive, since it avoids problems related to mass and charge conservation at fluid–solid interfaces, an artifact that has plagued previous LB implementations. It is then possible to model the dynamics of colloidal particles and polyelectrolytes in solution. The electrostatic interaction between them is derived from the charge distribution in the fluid. Hence, we do not need to assume any specific form for the interaction between charged colloids, or between monomers in a polyelectrolyte. Electro-osmosis, the sedimentation potential, electrophoresis, or other electrokinetic phenomena can be easily treated within the model. In this paper we consider the first two to illustrate the capabilities of the method.

The electrolyte is treated at the Poisson–Boltzmann level. We are not restricted to the linearized Debye–Hückel regime and can study the electrokinetic effects at high charge densities, being only limited by ionic condensation (as occurs, for example, in cylinders). The model we introduce will miss effects due to charge correlations.

The remainder of this paper is organized as follows: In Sec. II we describe the hydrodynamics of fluid mixtures to set the general background. In Sec. III we describe the proposed numerical method and, subsequently, in Sec. IV, we discuss how to model general solid interfaces within this lattice model. In Sec. V we focuses on the special case of interest to treat electrokinetic phenomena. In Sec. VI we validate the method by analyzing different situations of interest, including electro-osmosis, and sedimentation.

II. HYDRODYNAMIC DESCRIPTION OF NONIDEAL FLUID MIXTURES

In some respects, the dynamics of electrolytes at hydrodynamic scales is analogous to that of multicomponent mixtures. The simplest electrolyte model consists of two ionic species and a neutral solvent. In order to provide the general framework for the description of electrolyte dynamics, we first briefly review the dynamics of mixtures on hydrodynamic length and time scales. As in all hydrodynamic descriptions, the starting point of any discussion are the laws of conservation of mass and momentum.

A. Mass conservation

Every species of the fluid mixture satisfies the usual mass conservation law:

$$\frac{\partial \rho_k}{\partial t} + \nabla \cdot \rho_k \mathbf{v}_k = 0, \tag{1}$$

where $\mathbf{v}_k$ is the velocity and ρ_k the density distribution of the species labeled by k. The total density, $\rho = \Sigma_k \rho_k$, is also conserved, and satisfies an equation analogous to Eq. (1) with respect to the barycentric velocity $\rho \mathbf{v} = \Sigma_k \rho_k \mathbf{v}_k$, which describes the evolution of a fluid element. If we refer the motion of all species to this common velocity, then Eq. (1) can be expressed as

$$\frac{\partial \rho_k}{\partial t} + \nabla \cdot \rho_k \mathbf{v} = -\nabla \cdot \mathbf{j}_k, \tag{2}$$

where we have introduced the relative current of species k, $\mathbf{j}_k = \rho_k(\mathbf{v}_k - \mathbf{v})$, which accounts for all dynamical effects arising from the mismatch in velocities between the different species. On very short time scales, such currents are controlled by friction relaxation. However, for mixtures composed of molecular constituents (as is usually the case in electrolytes), the inertial time scale is extremely small; hence the relative current can be assumed proportional to a thermodynamic driving force, which is proportional to the gradient of the chemical potential. As a result, the relative current of species i becomes diffusive and can be expressed as[9]

$$\mathbf{j}_k = -\sum_k D_{ik} \rho_k \nabla \beta \mu_k, \tag{3}$$

where β is $1/k_B T$, with k_B the Boltzmann constant and $1/T$ the inverse temperature. $\beta \mu_k = \log \rho_k + \beta \mu_k^{\mathrm{ex}}$ is the chemical potential decomposed in an ideal and excess part, while D_{ik} corresponds to the diffusion coefficient that determines the flux of species i induced by spatial variations in the chemical potential of species k. For the sake of simplicity, we concentrate on the case where cross diffusion is neglected, and hence $D_{ik} = D_i \delta_{ik}$. By substituting the chemical potential in Eq. (3), we can then express mass conservation in the form of a set of convection-diffusion equations, expressing the two mechanisms that control the density evolution for each species,

$$\frac{\partial \rho_k}{\partial t} + \nabla \cdot \rho_k \mathbf{v} = \nabla \cdot D_k [\nabla \rho_k + \rho_k \nabla \beta \mu_k^{\mathrm{ex}}]. \tag{4}$$

B. Momentum conservation

Next, we consider momentum conservation. On the same length and time scales, momentum conservation implies that the barycentric velocity follows the Navier–Stokes equation:

$$\frac{\partial}{\partial t} \rho \mathbf{v} + \nabla \cdot \rho \mathbf{v} \mathbf{v} = \eta \nabla^2 \mathbf{v} + \xi \nabla (\nabla \cdot \mathbf{v}) - \nabla p + \mathbf{F}^{\mathrm{ext}}, \tag{5}$$

where η and ξ are the shear and bulk fluid viscosities, respectively, while $\mathbf{F}^{\mathrm{ext}}$ is the external force acting on a fluid element. The effect of the interactions among the different species enters as a net force expressed as the gradient of the local pressure, p. In the presence of spatial gradients, the pressure has, in general, a tensorial character, and can be derived from the free energy of the system. However, for

ideal electrolytes, the local pressure can always be expressed as a scalar. Hence, for the sake of simplicity we will consider this situation in what follows. As a result, we only need to input the free energy of the mixture to determine both the pressure and chemical potentials. Specifically, if we know the free energy per unit volume $\beta f(\mathbf{r})=\Sigma_k \rho_k[\log(\Lambda^3\rho_k)-1]+\beta f^{\mathrm{ex}}$, then

$$\beta\mu_k = = \log\rho_k + \beta\mu^{\mathrm{ex}},$$
$$\beta p = \sum_k \rho_k \beta\mu_k - \beta f = \sum_k (\rho_k + \rho_k \mu_k^{\mathrm{ex}}) - \beta f^{\mathrm{ex}}, \tag{6}$$

where the free energy, the chemical potential, and the pressure are position dependent. The first term of the pressure corresponds to the ideal-gas contribution, $\beta p^{\mathrm{id}}=\Sigma_k \rho_k$ while the other two contain all the information of the interactions among the fluid species. If there is one majority neutral component, which only contributes to the ideal part of the pressure, then the excess component of the pressure can be identified as the osmotic pressure of the mixture. In general, the pressure gradient follows from Gibbs–Duhem:

$$\beta\nabla p = \sum_k \rho_k \beta\nabla\mu_k = \sum_k (\nabla\rho_k + \rho_k\beta\nabla\mu_k^{\mathrm{ex}}), \tag{7}$$

and acts as a force. We will use this interpretation in the LB implementation discussed in the next section.

Using the last expression for the pressure gradient, the Navier–Stokes equation reads as

$$\frac{\partial}{\partial t}\rho\mathbf{v} + \nabla\cdot\rho\mathbf{v}\mathbf{v} = \eta\nabla^2\mathbf{v} + \xi\nabla\nabla\cdot\mathbf{v} - \nabla p^{\mathrm{id}} - \sum_k \rho_k \nabla\beta\mu^{\mathrm{ex}} + \mathbf{F}^{\mathrm{ext}}. \tag{8}$$

III. NUMERICAL LATTICE METHOD

We propose a model that combines a description of momentum dynamics based on lattice Boltzmann, with a numerical description of the convection-diffusion equation. Quantities are defined on the nodes of a lattice, $\mathbf{r}$, and time evolves in discrete time steps. The lattice is prescribed by specifying its connectivity. The connections of each node are determined by specifying the set of allowed velocities, $\mathbf{c}_i$, where the subindex i runs over all the allowed velocities. Then, each node $\mathbf{r}$ is connected to the nodes $\mathbf{r}+\mathbf{c}_i$.

A. Diffusion model

For convenience, let us rewrite the convection-diffusion equation, Eq. (4), in the form

$$\frac{\partial}{\partial t}\rho_k + \nabla\cdot\rho_k\mathbf{v} = -\nabla\cdot\mathbf{j}_k, \tag{9}$$

where the diffusive flux is

$$\mathbf{j}_k = -D_k(\nabla\rho_k + \rho_k\nabla\beta\mu_k^{\mathrm{ex}}). \tag{10}$$

For the sake of clarity, we discuss separately the change in density of the species k due to diffusion and to advection. The total change in time of the density is simply the sum of the two contributions.

1. Diffusion

Let us assume for the time being that the mixture diffuses in a fluid at rest. Equation (9) then becomes

$$\frac{\partial}{\partial t}\rho_k = -\nabla\cdot\mathbf{j}_k. \tag{11}$$

Integrating both sides of this equation over a volume V_0 and using the Green's formula $\int_{V_0}\nabla\cdot\mathbf{j}\,dV=\oint_{A_0}\mathbf{j}\cdot\hat{\mathbf{n}}\,dA$, we obtain

$$\frac{\partial}{\partial t}\int_{V_0}\rho_k\,dV = -\oint_{A_0}\mathbf{j}_k\cdot\hat{\mathbf{n}}\,dA, \tag{12}$$

where $\hat{\mathbf{n}}$ is the outward unity vector normal to the surface, A_0, enclosing the volume V_0.

As we have pointed out previously, we will consider densities defined on nodes of a lattice and the time evolution evolves at constant time steps. In this case, we can identify the volume V_0 with the volume associated to that node, and A_0 is related to the connectivity of the lattice nodes. Then, Eq. (12) states that the change of the total number of particles enclosed in the volume corresponding to node $\mathbf{r}$ equals the sum of the outward fluxes. Such fluxes can only take place by mass transport to the neighboring nodes that are connected to the central node, according to the structure of the predetermined lattice connectivity. Hence,

$$n_k(\mathbf{r},t+1) - n_k(\mathbf{r},t) = -A_0\sum_i j_{ki}(\mathbf{r}), \tag{13}$$

where $n_k(\mathbf{r})$ is the number of particles of species k at node $\mathbf{r}$, while $j_{ki}(\mathbf{r})$ accounts for the fraction of particles of species k going to node $\mathbf{r}+\mathbf{c}_i$. If we consider the velocity moving opposite to i, i.e., $\mathbf{c}_{i'}=-\mathbf{c}_i$, we have $j_{ki}(\mathbf{r})=-j_{ki'}(\mathbf{r}+\mathbf{c}_i)$ because these fluxes are always defined considering that the particles move away from the reference node. This unambiguously show that the fluxes are related to the links joining the connected nodes, rather than being quantities defined on the nodes.

It is worth noting that in the previous balance equation the relevant quantity is the number of particles of species k at node $\mathbf{r}$, $n_k(\mathbf{r})$, rather than its number density, $\rho_k(\mathbf{r})$. If we take the volume of a cell as our unit of volume, then $\rho_k(\mathbf{r})=n_k(\mathbf{r})$. However, in the presence of solid boundaries this distinction may become relevant. The prefactor A_0 in Eq. (13) is related to the geometrical structure of the lattice. Rather than connecting it directly with the area of the Wigner–Seitz cell that can be associated to node $\mathbf{r}$, we derive its magnitude by computing how density diffuses to the neighboring nodes. In Sec. VI A we will compute explicitly this geometric prefactor for a particular lattice. In the following, when referring to link mobility, we will use the symbol $d_k=D_kA_0$.

Using link fluxes to compute the variation of the densities of the different species avoids approximating the divergence on a lattice, a source of lattice artifacts, and the related potential spurious fluxes that may appear. Moreover, the use of these link fluxes also imposes locally mass conservation to machine accuracy, avoiding the errors caused by the discretization of the spatial gradient operator. We must still provide a prescription to implement the diffusive fluxes. These are, in

principle, given by Eq. (10) and involve spatial gradients between two neighboring lattice nodes. In equilibrium, $n_k^{\mathrm{eq}} \sim \exp[-\beta\mu^{\mathrm{ex}}]$ and, as a consequence, Eq. (10) predicts that all diffusive fluxes vanish. However, the direct implementation of Eq. (10) on a lattice will suffer from discretization errors that will result in small but noticeable spurious fluxes. To eliminate this effect, it is convenient to write the expression for the flux on a link as

$$\mathbf{j}_k(\mathbf{r},t) = -D_k e^{-\beta\mu_k^{\mathrm{ex}}(\mathbf{r},t)} \nabla[\rho_k(\mathbf{r},t) e^{\beta\mu_k^{\mathrm{ex}}(\mathbf{r},t)}], \tag{14}$$

because, in this expression, the gradient becomes identically zero when the density distribution corresponds to its equilibrium form. This also holds for the discretized form to be discussed below. Consistent with the idea that the flux can be expressed in terms of link mass fluxes, we propose a symmetrized implementation of j_{ki} involving magnitudes defined in the two connected nodes, $\mathbf{r}$ and $\mathbf{r}+\mathbf{c}_i$. In particular, we write the flux of species k along the link $\mathbf{c}_i$ as

$$j_{ki}(\mathbf{r}) = -d_k \frac{e^{-\beta\mu_k^{\mathrm{ex}}(\mathbf{r})} + e^{-\beta\mu_k^{\mathrm{ex}}(\mathbf{r}+\mathbf{c}_i)}}{2} \times \left[\frac{n_k(\mathbf{r}+\mathbf{c}_i) e^{\beta\mu_k^{\mathrm{ex}}(\mathbf{r}+\mathbf{c}_i)} - n_k(\mathbf{r}) e^{\beta\mu_k^{\mathrm{ex}}(\mathbf{r})}}{\Delta_i} \right], \tag{15}$$

where $\Delta_i = |\mathbf{c}_i| = |\mathbf{c}_{i'}|$ is the distance between the two neighboring nodes. This symmetrized formulation ensures that, to machine accuracy, $j_{ki}(\mathbf{r}) = -j_{ki'}(\mathbf{r}+\mathbf{c}_i)$, and mass is conserved for the model elementary dynamic processes. Note that, based on the mass conservation expression, Eq. (13), the global mass change of node $\mathbf{r}$ is the sum of the link fluxes, j_{ki}. Mass evolution in the diffusive limit is described only on the basis of mass flux divergence, as we have described. In general, the procedure developed based on link fluxes provides a consistent framework to obtain other gradients if needed.

2. Advection

Local density can also be altered due to advection if there is a local velocity of the fluid. If, for the time being, we disregard diffusion, the advection mechanisms can be written in the form

$$\frac{\partial}{\partial t}\rho_k = -\nabla\cdot(\rho_k \mathbf{v}), \tag{16}$$

where $\mathbf{v}$ is the barycentric fluid velocity. In principle, the change in the number of particles could be computed on the basis of the advection along each link, in a way similar to Eq. (13). However, as we will describe in the next section, the model we will introduce provides the velocity at each node, rather than the link velocity. In order to avoid numerical artifacts and spurious diffusion due to the interpolation to get such a link velocity, we propose an alternative implementation of the advection process. We still consider that $n_k(\mathbf{r})$ give us the number of particles in a volume element centered around node $\mathbf{r}$. Since we know the velocity of that node, $\mathbf{v}(\mathbf{r})$, in one step the node will *virtually* displace to $\mathbf{r}+\mathbf{v}(\mathbf{r})$. As a result, the volume associated to node $\mathbf{r}$ will intersect some neighboring cells of the real lattice (see Fig. 1). We then distribute the amount of particles n_k into the intersected volumes proportionally to the intersected region. In Fig. 1, we depict in shadow the volumes that correspond to the fraction of the density that is transported in the new cells. The advantage of this approach is that it greatly reduces the spurious diffusion that usually results during advection in lattice models. To be more precise, even with the present method, advection will cause some spurious diffusion (proportional to the flow velocity). However, in Sec. VI A we show that, in practice, this effect is negligible.

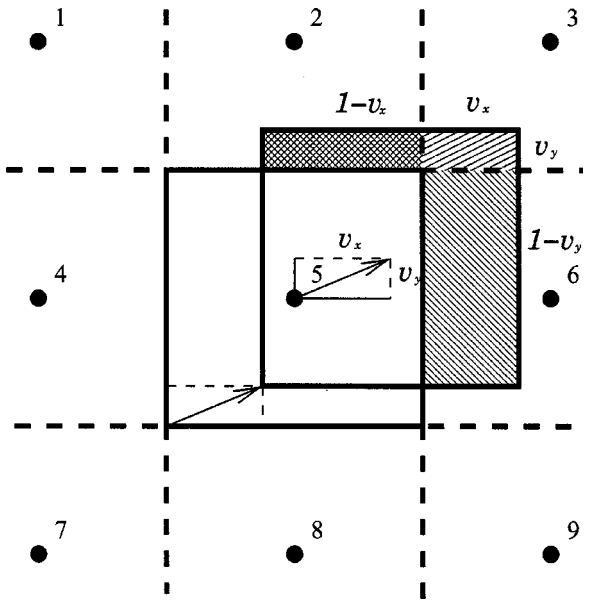

FIG. 1. Density redistribution due to advection. To advect the charge of a given node (in this case, node number 5) in one time unit, we shift the whole cell with the local velocity vector of that node (v_x, v_y). Next, we displace a fraction of density equal to the area of the cell that is now in the corresponding site. In the graph a fraction of the density equal to the shadowed rectangle area $(v_x v_y)$ goes from cell 5 to cell 3, a fraction $(1-v_x)v_y$ goes to cell 2, $(1-v_y)v_x$ goes to cell 6, and $(1-v_x)(1-v_y)$ stays at node 5. For the sake of clarity, the figure shows a two-dimensional flow. In practice, the analogous procedure is carried out in 3D.

B. Lattice Boltzmann method

In order to simulate the hydrodynamic flow of the fluid, we make use of the lattice-Boltzmann approach. This technique has been used extensively to model hydrodynamic flows in complex geometries.[10] It is equivalent to solving a discretized version of the Boltzmann equation with a linearized collision operator. This method describes the dynamics of a fluid in terms of the densities of particles that ''live'' on the nodes of a cubic lattice and have discrete velocities $\{\mathbf{c}_i\}$, where i labels the links between a lattice point $\mathbf{r}$ and its neighbors. The values of the velocities are chosen such that, in one time step, a particle moves along a link from one lattice node to its neighbor. In the lattice-Boltzmann model, the unit of length is equal to the lattice spacing and the unit of time is equal to the time step. In addition, the unit of mass (or, equivalently, energy) is fixed by the requirement that, in the continuum limit, the transport equations for the lattice model approach the Navier–Stokes equation. This imposes a relation between the temperature and the speed of sound [see

below Eq. (20)]. The central dynamic quantity in the lattice-Boltzmann approach is the one-particle distribution function, $f_i(\mathbf{r},t)$, which describes the probability of having a particle at site $\mathbf{r}$ at time t with velocity $\mathbf{c}_i$. The hydrodynamic variables are obtained as moments of this distribution function over the lattice velocities, $\mathbf{c}_i$; e.g., density and momentum can be obtained as

$$\rho(\mathbf{r},t)=\sum_i f_i(\mathbf{r},t),$$
$$\mathbf{j}(\mathbf{r},t)\equiv\rho(\mathbf{r},t)\mathbf{v}(\mathbf{r},t)=\sum_i \mathbf{c}_i f_i(\mathbf{r},t), \tag{17}$$

respectively.

In the presence of external forces, $\mathbf{F}$, the evolution equation can be expressed as

$$f_i(\mathbf{r}+\mathbf{c}_i,t+1)=f_i(\mathbf{r},t)+\mathcal{L}_{ij}[f_j(\mathbf{r},t)-f_j^{\mathrm{eq}}(\mathbf{r},t)]+\psi_i, \tag{18}$$

where $\mathcal{L}[\Psi]$ is a linear collision operator acting on Ψ that tends to relax the distribution function toward its equilibrium limit. Hence, one needs to specify the equilibrium distribution as well as the collision operator. The collision operator ensures mass and momentum conservation (i.e., $\Sigma_i\mathcal{L}_{ij}=\Sigma_i\mathbf{c}_i\mathcal{L}_{ij}=0$). Its eigenvalues also determine the viscosity of the fluid. The equilibrium distribution appearing in Eq. (18) is that of an ideal gas. It can be shown that the Navier–Stokes equations are recovered, keeping a low-velocity expansion of the Maxwellian,[10] i.e.,

$$f_i^{\mathrm{eq}}=a^i\left[\rho+\frac{1}{c_s^2}\mathbf{c}_i\cdot\mathbf{j}+\frac{1}{2c_s^4}\rho\mathbf{vv}:(\mathbf{c}_i\mathbf{c}_i-c_s^2\mathbf{1})\right], \tag{19}$$

where: is the double inner product, and the coefficients a^i, depend on the geometry of the lattice, and are chosen to ensure that the anisotropy of the lattice does not affect the hydrodynamic behavior of the model, as well as ensuring that all the distribution functions are non-negative. Moreover, c_s is the speed of sound and its value depends on the values of the coefficients a^i, but it is always smaller than unity (in lattice units). Finally, the term ψ_i accounts for the external force. It satisfies $\Sigma_i\psi_i=0$ and $\Sigma_i\mathbf{c}_i\psi_i=\mathbf{F}$. For a more detailed description of how to model the external force, see, e.g., Refs. 11 and 12.

By means of a Chapman Enskog expansion, it can be shown[11] that in the hydrodynamic limit one recovers the Navier–Stokes equation,

$$\frac{\partial}{\partial t}\rho\mathbf{v}+\boldsymbol{\nabla}\cdot\rho\mathbf{vv}=\eta\nabla^2\rho\mathbf{v}+\xi\boldsymbol{\nabla}\boldsymbol{\nabla}\cdot\mathbf{v}-c_s^2\boldsymbol{\nabla}\rho+\mathbf{F}. \tag{20}$$

Since the third term on the rhs is the pressure gradient for an ideal gas, if we fix the temperature such that $k_{\mathrm{B}}T=c_s^2$, we then recover Eq. (5) for an ideal mixture. For nonideal mixtures, we will introduce the missing contribution to the pressure gradients as a local external force, $\mathbf{F}$. Because the solutes act onto the solvent exclusively by means of this effective force $\mathbf{F}$, the hydrodynamic limit of the non-ideal-mixture model is obtained by following the same procedure as the one needed for the standard lattice Boltzmann method for one phase flows.[11]

Introducing the mixture nonideality as a local effective force implies that the fluid reacts with the appropriate susceptibility to applied external fields, although in the absence of spatial gradients the equilibrium distribution corresponds to that of an ideal gas. Since we are not concerned with local structure, the model can be regarded as an effective kinetic model, similar in structure to a linearized Vlasov equation. Hence, this approach differs from previous proposals that try to derive the hydrodynamics of nonideal mixtures from kinetic models of mixtures[13] or from a modification of the equilibrium distribution to recover the equilibrium pressure.[8]

For a particular choice of the shear viscosity, $\eta=1/6$ in lattice units,[14] the general dynamic rule Eq. (18) simplifies to

$$f_i(\mathbf{r},t+1)=a^i\left[\rho(\mathbf{r},t)+\frac{1}{c_s^2}\mathbf{c}_i\cdot(\mathbf{j}(\mathbf{r},t)+\mathbf{F})+\frac{1}{2c_s^4}\rho\mathbf{vv}:(\mathbf{c}_i\mathbf{c}_i-c_s^2\mathbf{1})\right]. \tag{21}$$

For the sake of convenience, we implement the model with this simplified updating rule. However, it is straightforward to implement the more general form that allows us to impose other values of the viscosity.

The peculiarities of the nonideality of the mixture enters through the forcing term ($\mathbf{F}$) in Eq. (21). This forcing term can be decomposed into an external field and a interaction contributions, $\mathbf{F}=\mathbf{F}^{\mathrm{ext}}+\mathbf{F}^{\mathrm{sol}}$. This interaction force, as previously described in Eq. (7), has the form $\mathbf{F}^{\mathrm{sol}}=\Sigma_k\rho_k\nabla\beta\mu_k^{\mathrm{ex}}$. Using the same approach that we have used to model the convection-diffusion equation, we can determine the force acting on each link, F_i. Moreover, for the particular case where the diffusion matrix is diagonal,

$$F_i(\mathbf{r})=\sum_k\left[\frac{j_{ki}}{D_k}-\frac{n_k(\mathbf{r}+\mathbf{c}_i)-n_k(\mathbf{r})}{\Delta_i}\right]. \tag{22}$$

The advantage of using the force exerted on the links is that, again, we keep a symmetric dependence on the neighboring nodes, and, moreover, $F_i(\mathbf{r})=-F_{i'}(\mathbf{r}+\mathbf{c}_i)$. Yet, in the lattice-Boltzmann update rule, we need the force acting on the node. This force can be obtained averaging the link forces,

$$F_\alpha^{\mathrm{sol}}(\mathbf{r})=\sum_i a^i c_{i\alpha}F_i(\mathbf{r}),\quad \alpha=x,y,z. \tag{23}$$

Let us now introduce an alternative way of treating the same systems. There are situations, as is the case in electrolytes, where one of the components of the mixture is dominant, and plays the role of the solvent. In this case, we can single out this component, ρ_s, and treat it separately from the rest. In particular, since $\rho_s\gg\rho_k$, we can approximate the overall density by the solvent density ($\rho\simeq\rho_s$), and the overall momentum by the solvent momentum ($\rho v=\Sigma_k\rho_k v_k\simeq\rho_s v_s$). If we then relate the moments of the distribution function f_i to the solvent density, i.e., $\Sigma_i f_i=\rho_s$ and $\Sigma_i\mathbf{c}_i f_i=\rho_s\mathbf{v}_s$ instead of Eqs. (17), we impose a constant solvent

density in the incompressible regime. Hence, the rest of the components will need to compensate their densities to avoid any net local density variation. Although this incompressibility constraint is not exact, it may be a convenient approximation. From the point of view of the link force, Eq. (22), it has the computational advantage that one gets $F_i = \Sigma_k j_{ki}/D_k$ and it reduces to the link diffusive flux previously computed, Eq. (15). In this case the Navier–Stokes equation becomes

$$\frac{\partial}{\partial t}\rho_s \mathbf{v}_s + \boldsymbol{\nabla}\cdot\rho_s \mathbf{v}_s \mathbf{v}_s = \eta \nabla^2 \mathbf{v}_s + \xi \boldsymbol{\nabla}\boldsymbol{\nabla}\cdot\mathbf{v}_s - c_s^2 \boldsymbol{\nabla}\rho_s - k_B T \sum_k [\boldsymbol{\nabla}\rho_k + \boldsymbol{\nabla}\mu_k^{\mathrm{ex}}] + \mathbf{F}^{\mathrm{ext}}, \tag{24}$$

and by taking $k_B T = c_s^2$, we recover an appropriate behavior when $\rho_s \gg \rho_k$.

The advantage of this approach is that densities of different species are dealt with on different footing, which may prove advantageous in certain applications, especially when dealing with boundary conditions that act differently on the solvent and solute, as it is the case if dealing with semipermeable membranes. Numerically, in this case there is a net force only when the density distribution deviates from its local equilibrium value, in contrast with the original method, where the density coming from the advection contribution balances the local force. This ensures an additional way to avoid spurious artifacts from the underlying lattice.

IV. BOUNDARY CONDITIONS

If the fluid mixture is confined between walls, or if colloids are added to the mixture, we need to specify how the densities and distribution function will interact with solid interfaces. To account fully for such an interaction, we need to describe in turn how the distribution function behaves, how the particle number evolves, and how we estimate the interacting force at the surface.

At a solid surface we expect hydrodynamic ''stick'' boundary conditions to apply. One way to impose these is to apply the so-called ''bounce-back rule'' on the links. However, the standard version of this procedure (see, for example, Ladd[11]) allows the fluid to leak into the solid. Although this leakage is usually innocuous, there are cases (a typical example being when electrostatics is part of the excess chemical potential) where this leakage may change the density of the solvent inside the solid, leading to a corresponding error in the pressure gradient. There exist alternative bounce-back rules that do not allow for any fluid leakage.[15]

The formulation of our model in terms of link fluxes simplifies the implementation of boundary conditions for the fluxes of the different species densities, ρ_k. Since the convection-diffusion equation involves only mass conservation, it is enough to impose that there is no net flux on any link that joins a fluid node and a solid node. We accomplish this by imposing that the diffusive flux $j_{ki}=0$ on such a link, and that the flux due to advection also vanishes. This second requirement is achieved by a kind of partial bounce-back move: the number of particles that would have been assigned to a solid node after advection is reflected back to its node of origin.

The updating rule, both for the number densities of the convection-diffusion equations and for the lattice Boltzmann distribution function, requires the evaluation of gradients of chemical potentials. To this end, we need to specify the values of the excess chemical potentials on neighboring nodes, and those may involve the values of the fluid densities in contact with the solid wall. We consider that the relevant value of the density is that in contact with the wall, which is somewhere in between the fluid and the solid node. Such value can be obtained by requiring that it is consistent with the no-flux condition for the link flux of that species. The no flux condition is satisfied, requiring [see Eq. (15)]

$$n_k(\mathbf{r}+\mathbf{c}_i) = n_k(\mathbf{r}) e^{\beta[\mu_k^{\mathrm{ex}}(\mathbf{r}+\mathbf{c}_i) - \mu_k^{\mathrm{ex}}(\mathbf{r})]}, \tag{25}$$

which should be understood as the extrapolation of the fluid density to ensure the absence of flux diffusion, and, in general, it is an implicit equation to obtain an estimate of the extrapolated number of particles, $n_k(\mathbf{r}+\mathbf{c}_i)$. Note that this fictitious extrapolated density is a property of the link, not of the node.

As we have mentioned in Sec. III, the formulation based on the fluxes is based on the evolution of the number of particles contained in a given volume element. For the fluid nodes in the absence of solid interfaces the particle number is proportional to the number density. This is no longer the case close to a solid wall. This difference is pertinent because the excess chemical potential and the pressure are functions of the number density, ρ_k. While for a wall at rest, one can still consider that the wall is equidistant from the nodes and n_k and ρ_k coincide, for a moving solid surface, the position of the solid boundary will change as it moves. In this case, a coefficient α that establishes how close the solid boundary is to the fluid node should be introduced. In the limiting case that the solid boundary is reaching the neighboring fluid node, the corresponding cell has a volume that is approximately half the volume of a usual cell, hence $\alpha=1/2$; in the opposite case when the solid surface reaches the solid node one gets accordingly $\alpha=3/2$. This coefficient then allows us to relate $n_k=\alpha\rho_k$. Although there exist different ways in which this coefficient may be computed, any smooth function that accounts for the volume change will be enough to avoid abrupt changes in the density when a fluid nodes is absorbed or created by the moving boundary.

V. ELECTROKINETIC EQUATIONS

In the previous sections we have developed a model to simulate general nonideal fluid mixtures. We will now analyze the special case in which the fluid mixture is an electrolyte. The simplest electrolyte model corresponds to a three-species mixture, two of them being the ionic species, ρ_+ and ρ_- with charges z_+e and z_-e, and the third one being the neutral solvent ρ_s. e is the elementary charge, and z_+ and z_- are the valencies of the ions. The local charge can then be expressed as $q(\mathbf{r}) = e[z_+\rho_+(\mathbf{r}) + z_-\rho_-(\mathbf{r})]$. The simplest

free-energy model corresponds to an ideal mixture in the absence of any local electric field, where we can write

$$\beta f(\mathbf{r}) = \sum_{k=\pm,s} \rho_k [\log(\Lambda_k^3 \rho_k) - 1] + \frac{1}{2} \beta q \hat{\Phi}, \tag{26}$$

with $\hat{\Phi}$ being the electrostatic potential and the factor 1/2 avoids double counting. The chemical potential is then

$$\beta \mu_k = \log \rho_k + \beta z_k \hat{\Phi}, \quad k = +, -,$$

$$\beta \mu_s = \log \rho_s .$$

The hydrodynamic evolution equations for this free energy model become

$$\frac{\partial}{\partial t} \rho_k + \boldsymbol{\nabla} \cdot \rho_k \mathbf{v} = D_k \boldsymbol{\nabla} \cdot [\boldsymbol{\nabla} \rho_k + e z_k \rho_k \boldsymbol{\nabla} \beta \hat{\Phi}] \tag{27}$$

$$\frac{\partial}{\partial t} \rho \mathbf{v} + \boldsymbol{\nabla} \cdot \rho \mathbf{v} \mathbf{v} = \eta \nabla^2 \rho \mathbf{v} + \xi \boldsymbol{\nabla} \boldsymbol{\nabla} \cdot \rho \mathbf{v} - c_s^2 \boldsymbol{\nabla} \rho + \beta \sum_k e z_k \rho_k \boldsymbol{\nabla} \hat{\Phi}. \tag{28}$$

We still need an additional equation that prescribes how the electrostatic potential is related to the local charge density. Since transport processes associated to mass and momentum transfer in fluid mixtures are much slower than the propagation of electromagnetic waves, the electric field is completely determined by the Poisson equation,

$$\nabla^2 \Phi = -4 \pi l_B \left[\sum_{k=\pm} z_k \rho_k + \rho_s \right], \tag{29}$$

which has been expressed in terms of a dimensionless potential, $\Phi = e \beta \hat{\Phi}$, while $l_B = \beta e^2 / (4 \pi \epsilon)$ is the Bjerrum length (the distance at which the electrostatic and the thermal energies are equal), with ϵ the dielectric constant of the fluid. In the previous equation, ρ_s stands for the charge density of the solid surfaces, if there are confining walls or moving suspended particles in the electrolyte. Obviously, σ will be nonzero only on those solid surfaces. The equations (27), (28), and (29) are commonly referred to as the Electrokinetic equations.

The electrostatic potential Φ can be computed using standard techniques. Specifically, we have implemented a successive over-relaxation scheme (SOR),[16] as described in more detail in Ref. 7. The advantage of this model is that it does not presume a specific type of boundary condition, and can be easily generalized to deal with media of different dielectric constants. Although not as fast as other methods for solving the Poisson equation, it is adequate for our purposes because, once the local equilibrium charge profiles are achieved, the calculation of the disturbed electrostatic potential due to external forces is much less time consuming than the iteration part related to lattice Boltzmann and convection diffusion; alternative, more sophisticated, variants to solve the Poisson equation numerically can be implemented wherever the standard SOR routine proposed here becomes unpractical.

VI. VALIDATION TESTS

In order to validate the model that we introduced in the previous section, we compare its predictions against known results. In particular, we verify that the equilibrium charge distribution is properly recovered on the lattice, and that out of equilibrium the different coupling mechanisms between fluid flow and charge inhomogeneities are properly accounted for.

A. Effective diffusion

As was pointed out below Eq. (13), the diffusion coefficient characterizing the discrete version of the diffusion equation is not the same as the link diffusion coefficient, d_k, but is related to it through a simple geometrical factor A_0 that depends on the type lattice used. A_0 can be evaluated as follows. Consider a situation where the transport of species k is purely diffusive. A density perturbation ρ_0, initially localized at node $\mathbf{r}_0$, will spread in one time step to the connected neighboring nodes. If the process is purely diffusive, we know the amplitude of the second moment of the density variation during this time step and $\Sigma_i \Delta_i^2 \rho(\mathbf{r}_0 + \mathbf{c}_i, t_0 + 1) = 6 D_k \rho_0 = 6 A_0 d_k \rho_0$ in a three-dimensional cubic lattice. Let us consider for concreteness the D3Q18 lattice,[19] which is the lattice we used in our LB simulation. Since the link fluxes $j_i = d_k \rho_0 / \Delta_i$, after one time step the density in each of the six nearest neighbors is $d_k \rho_0$, while the density in each of the other 12 connected nodes is $d_k \rho_0 / \sqrt{2}$. As a result, $\Sigma_i \Delta_i^2 \rho(\mathbf{r}_0 + \mathbf{c}_i, t_0 + 1) = d_k (6 + 12\sqrt{2}) \rho_0$, which implies that $A_0 = 1 + 2\sqrt{2}$ [or $D_k = d_k (1 + 2\sqrt{(2)})$]. Depending on the value of d_k, it might happen that the total density transferred to the neighbors is larger than the initial density. For D3Q18 this gives us an upper bound for the input diffusion coefficient that ensures absolute stability, $d_k \leqslant 1/(6(1 + 2\sqrt{2})) = 0.044$. In practice, we find that for all cases that we have analyzed, numerical instabilities related to diffusion become relevant for values of the input diffusion coefficient $d_k \geqslant 0.05$. In order to perform simulations at higher diffusivities, we need to modify the numerical scheme to simulate the diffusion equation. This instability can be overcome by introducing a multiple-time step technique. To this end, we introduce a smaller diffusion coefficient $d_{it} = d_k / N_{it}$ and iterate N_{it} times the discrete diffusion equation, Eq. (13), to advance the densities one time step.

When applying this multiple time step method to solve the lattice diffusion equation, one must compute carefully the force that should be applied to the distribution function f_i at the end of the time step. In fact, $\mathbf{F}^{\mathrm{sol}}$ should be computed at all the intermediate steps. All these contributions should then be added to obtain the total force at the end of the iteration. With this technique we can vary the diffusion coefficient over several orders of magnitude. For example, in our simulations we could vary D_k from $D_k = 10^{-3}$ to $D_k = 6$ (all in lattice units).

On top of the lattice effects on diffusion itself, advection can also induce spurious diffusion, because the lattice velocities do not coincide, in general, with the local velocity. As a consequence, a concentrated set of particles will spread over the lattice nodes, even if subject to a pure translational mo-

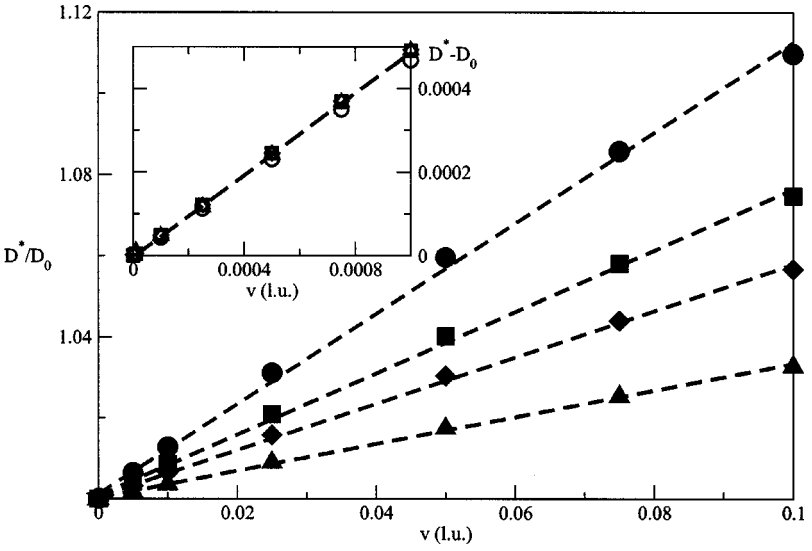

FIG. 2. In the lattice-Boltzmann model, advection causes some spurious diffusion. The figure shows the computed effective diffusion, D^*/D_0, as a function of the fluid velocity for the steady state described in Sec. III A 1. The curves are drawn for different diffusion coefficients at zero velocity: $D_0=0.38$ (circles), $D_0=0.57$ (squares), $D_0=0.76$ (diamonds), and $D_0=1.34$ (triangles). In the inset we show that the amount of diffusion induced by the flow does not depend on the equilibrium coefficient and has, for small velocities, a linear velocity dependence. Symbols are the simulation result and the dashed line corresponds to the theoretical expression described in the text.

tion. Hence, only when the velocity is commensurate with the lattice spacing, both in direction and magnitude, will spurious diffusion be exactly zero. We must then quantify the amount of spurious diffusion. To this end, we consider an ideal binary mixture composed of a solvent with initial uniform density, ρ_s, and a solute with initial density ρ_t. The mixture is contained between two parallel walls that are permeable to the solvent but impermeable to the solute. The fluid is moving with a uniform velocity v perpendicular to the walls. As a result of the impermeability of the walls to the solute, a steady state is reached, determined by the solvent density profile, $\rho_t(x)$, which satisfies

$$\rho_t(x)=\rho_0 \exp\left[-\frac{v}{D^*}(x-x_0)\right], \tag{30}$$

where v is the fluid velocity, D^* the effective diffusion coefficient, and ρ_0 the solvent distribution at contact with the wall located at x_0.

In Fig. 2 we show the effective diffusion coefficient measured by using Eq. (30) as a function of the fluid velocity for a range of values of the diffusion coefficient. We plot D^*/D_0 (where D_0 is the diffusion coefficient for a quiescent fluid). In order to show that there exists an intrinsic advection-induced spurious diffusion, we plot in the inset of the same figure the difference between the effective and the input diffusion coefficient for many values of the input diffusion coefficient as a function of the fluid velocity. Because all curves collapse, this graph shows that the diffusion coefficient induced by the advection depends only on the fluid velocity. We observe that the dependence on the (absolute value of) flow velocity is linear with slope 1/2. Following the procedure that we used above to compute the factor A_0, we can derive an expression for the advection-induced diffusion coefficient. In one dimension, a fraction $v\Delta t$ of the density $\rho(x)$ is displaced to the next node, while a fraction $(1-v)\Delta t$ remains at the original node. The center of mass of the density is displaced by a factor $v\Delta t$. Simple algebra then shows that the second moment of the density variation during a time step is $\langle \Delta_i^2 \rangle = v(1-v)$. The flow-induced diffusion coefficient in one dimension is therefore $D^*=(1/2)v-(1/2)v^2$. In three dimensions this expression is readily generalized to yield

$$D^*=\frac{1}{2}[v_x(1-v_x)+v_y(1-v_y)+v_z(1-v_z)]. \tag{31}$$

By choosing a sufficiently low value of the flow velocity, and a sufficiently large value of D_0, we can largely suppress the effect of this advective diffusion.

If, on the other hand, one is interested in large values of the Peclet number ($\mathrm{Pe}=vl/D$, where v and l are, respectively, a typical velocity and length of the system and D the diffusion coefficient of the solutes), Eq. (31) sets an upper limit. The smallest diffusion coefficient achievable is given by the spurious diffusion (we put the proper diffusion coefficient to zero). Then, by substituting the expression for the spurious diffusion into the definition of the Peclet number, we obtain

$$\mathrm{Pe}=\frac{vl}{D}\simeq\frac{vl}{\frac{1}{2}v-\frac{1}{2}v^2}=\frac{2l}{1-v}. \tag{32}$$

For reasons of flow stability, the quantity $1-v$ will always be of order 1. Therefore the maximum Peclet number achievable will be $\mathrm{Pe}\simeq 2l$. In other words, a tracer will be able to travel a distance twice the obstacle size without feeling any diffusion.

B. Electrolyte in a slit

Next, we consider a fluid confined between two parallel solid walls at rest, with a constant surface charge. The slit has a width L and the surface density charge is fixed to $\rho(-L/2)=\rho(L/2)=\sigma/2$.

The space between the two slits is occupied by a solvent and counterions. In order to achieve global neutrality, the density of the counterion is initially set to be uniformly distributed, $\rho(x)=-\sigma/L$, $x\in\{-L/2,L/2\}$.

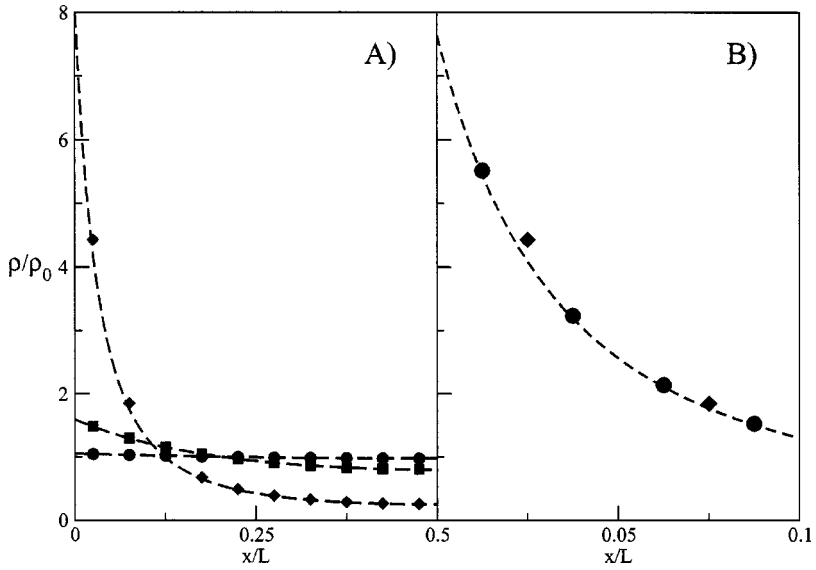

FIG. 3. Equilibrium distribution of the charge density of counterions (no added salt) in the slit between two charged walls at a distance L. The abscissa measures the distance from the wall in units of L. The local density is expressed in units of the average charge density in the bulk: $\rho_0=\sigma/L$. (a) charge distributions for three values of the dimensionless parameter KL (see the text): $KL=0.553$ (circles), $KL=1.57$ (squares), and $KL=2.77$ (diamonds). In the same figure, we have indicated the corresponding analytical results [Eq. (33)] (dashed curves) for a slit of width $L=20$ lattice spacings. Circles and squares correspond to the linear regime ($K/K_{\mathrm{lin}}=1.01$ and 1.13, respectively), while diamonds are close to the saturation limit ($K/K_{\mathrm{lin}}=2.01$). (b) The accuracy of the numerical solution for the charge profile can be improved by increasing the spatial resolution of the lattice, in this case from $L=20$ (diamonds) to $L=40$ (circles). Again, the analytical result is shown as a dashed curve. The curves in (b) correspond to the result for a highly charged surface, $KL=2.77$ ($K/K_{\mathrm{lin}}=2.01$).

The actual position of the hydrodynamic and electrostatic solid boundary cannot be resolved within a lattice spacing. In the neutral case, for the viscosity and geometry considered the wall can be assumed to be halfway between two consecutive lattice nodes, as dictated by the bounce-back rule.[14] We will use this position as a reasonable approximation. In fact, the results we describe for a planar slit indicate that for a planar wall the electrostatic position of the wall can be taken as being midway between the boundary nodes. For a nonplanar interface a separate calibration will be required.

1. Equilibrium distribution of the counterion density

In equilibrium, a uniform charge density on a flat wall will induce an inhomogeneous equilibrium density profile of the counterions. For this simple geometry, the charge-density profile of the counter ions is analytically known (at least, at the Poisson–Boltzmann level)[6,17] for an arbitrary surface charge density:

$$\rho(x)=\frac{\rho_0}{\cos^2(Kx)}, \tag{33}$$

where $\rho_0=K^2/2\pi l_{\mathrm{B}}$, K is the solution of the transcendental equation,

$$\frac{KL}{2}\tan\left(\frac{KL}{2}\right)=\pi l_{\mathrm{B}}L\sigma, \tag{34}$$

which involves the wall charge density. Since we have an exact solution for the full Poisson–Boltzmann equation for arbitrary values of the wall charge, this geometry is a good case to analyze the limitations of the model dealing with large charges, i.e., beyond the linear Poisson–Boltzmann limit. For low surface charge densities, the linear regime is recovered by linearizing Eq. (34), and the parameter K becomes $K_{\mathrm{lin}}L=\sqrt{4\pi l_{\mathrm{B}}\sigma}$.

In the opposite limit of high surface-charge density, K saturates at $K_{\mathrm{sat}}L=\pi$. We can then quantify the deviation of the fluid from the linearized regime, where the electrostatic interactions are small by analyzing the departure of KL from $K_{\mathrm{lin}}L$.

In Fig. 3(a) we show the equilibrium counterion distributions in both limits. In our simulations we fixed the Bjerrum length to be 0.4, the channel width to 20 lattice nodes, and we have varied the surface-charge density. In the plot we show the profiles for $K/K_{\mathrm{lin}}=1.01$, 1.13, and 2.01, which correspond to $\sigma=0.003\,125$, $0.031\,25$, and 0.3125 in dimensionless lattice units, respectively. The highest value of K is not far from the saturation value. The figure shows that, with the present method, we can indeed reproduce the correct counterion distribution, both in the linear and in the nonlinear regime. In Fig. 3(b) we compare the density profiles close to the wall in the nonlinear regime for two different slit widths. The larger the surface charge the more localized the charge profile will be. The figure shows that increasing the resolution of the lattice does result in a small but significant improvement in the calculation of the charge distribution. Of course, the discrepancy would be greater for a more localized charge profile. In practice, only the computer resources (memory) will set an upper limit for the surface charge density that can be modeled reliably with the present scheme.

2. Electro-osmotic flow

Having verified that the model correctly reproduces the equilibrium behavior, we next turn to the calculation of flow

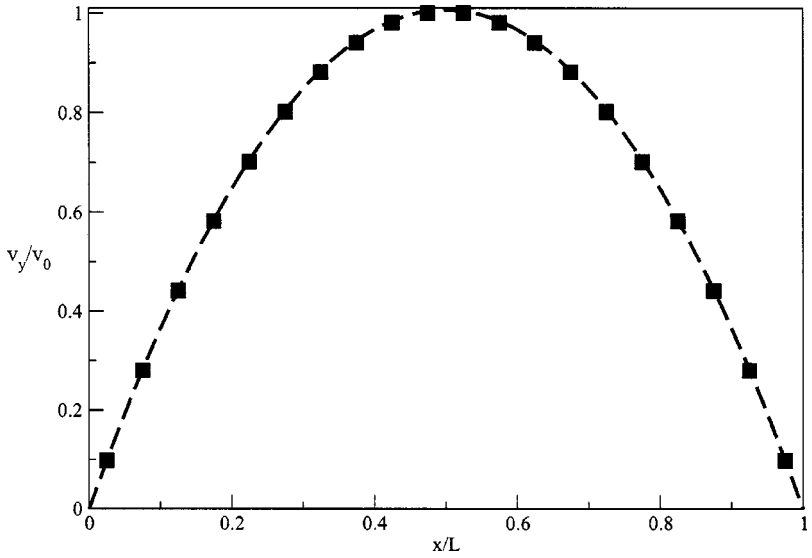

FIG. 4. Electro-osmotic flow profile in a slit of width $L=20$ lattice spacings. The surface charge density, $\sigma=0.003\,125$ ($K/K_{\mathrm{lin}}=1.01$), corresponds to the linear regime. The fluid in between the slit contains only counterions. The electric field is along the y direction. It has a strength of 0.1 in units $k_{\mathrm{B}}T/(\Delta l e)$, where Δl is the lattice spacing and e is the elementary charge. The simulation results are compared to the theoretical prediction, Eq. (35), shown as a dashed curve.

caused by an external electric field. We apply a constant external electric field that is parallel to the slit, $E^{\parallel}$. This field causes hydrodynamic flow as it exerts a force on those fluid elements that carry a net charge. If we take y as the component along the walls and refer to x as the coordinate perpendicular to the walls, then, at the Poisson–Boltzmann level, the exact solution for the fluid flow in the steady state can be written as[6]

$$v_y(x)=\frac{eE^{\parallel}\rho_0}{\eta K^2}\log\left[\frac{\cos(Kx)}{\cos\left(\frac{KL}{2}\right)}\right], \tag{35}$$

where η is the shear viscosity of the fluid. In our simulations, we model the constant electric field by taking into account the potential difference that it causes between neighboring lattice nodes [i.e., $\Delta\hat{\Phi}_{\mathrm{ext}}(y)=E^{\parallel}\Delta y$].

Figure 4 shows the computed electro-osmotic flow profile in a slit confined by hard walls with a charge density $\sigma=0.003\,125$ (in units of the elementary charge per square lattice unit). In the same figure, we also show the analytical solution [Eq. (35), with $K/K_{\mathrm{lin}}=1.01$] that is exact in the Debye–Hückel limit. Again, there is good agreement between theory and simulation. This suggests that the effect of electrostatic forces on the hydrodynamic flow is correctly taken into account in the simulations.

C. Sedimentation velocity

In the previous sections we have seen that the appropriate equilibrium charge distribution is reproduced both in the linear and nonlinear regimes of the Poisson–Boltzmann equation, and that also a charge distribution induces the correct fluid profiles. We must still show that the opposite coupling works correctly, i.e., we must compute the hydrodynamic drag on a charged object, in the absence of external electrical fields.

To this end, we compute the sedimentation velocity of an array of charged spheres immersed in an electrolyte solution. In this case, the velocity of the colloidal particle induces a fluid flow that determines the steady charge distribution around the sphere. This charge distribution, in turn, affects the sedimentation velocity of the particle. Hence, all the different couplings between charge, electrostatic potential, and fluid flow are present. Such a scenario has been analyzed previously with a different model[7] and analytically at infinite dilution.[18] As a consequence, we can again check our simulations against known results.

The system that we consider consists of a charged sphere of radius a in a three-dimensional box of size L. Because of periodic boundary conditions, this corresponds to a periodic array of spheres with volume fraction $\varphi=(4\pi a^3/L^3)$. In the simulation, we first allow the electrolyte to equilibrate with the particle at rest in the absence of external forces; hence the system develops its equilibrium double layer. Then, we apply the gravity as an external body force applied to the fluid, i.e., we move in the system of reference of the colloid. In this way we avoid the problem of updating the particle's position due to its motion.[19] By forcing the colloid to be at rest, we will not conserve momentum, but by computing the mean fluid velocity in the steady state (which is reached on a time scale of order $L^2\rho/\eta$), we can obtain the sedimentation velocity.

We have fixed the Bjerrum length to $l_{\mathrm{B}}=0.4$ and the radius of the sphere to $a=4.5$ in lattice units. We performed calculations for two different values of the solvent fluid density, $\rho_s=1$, and $\rho_s=20$, while the density of the added salt ρ_k was varied between 1.8×10^{-2} and 4×10^{-4}. As we vary the salt concentration, we also change the Debye length from 3.3 to 21. In order to be sure that the equilibrium properties were correct, we have computed the co- and counterion equilibrium density distributions and found very good agreement with the ones predicted by the Debye–Hückel theory for all the Debye lengths considered. In particular, spheres with radius 4.5 lattice units are well described by their approximate lattice representation. Since $\rho_s\gg\rho_k$, we have performed most calculations using the second version of our simulation scheme, as described at the end of Sec. III B. However, we also performed some simulations using the original model (taking the solvent density as the overall density). The only difference that we observe between the two implementations

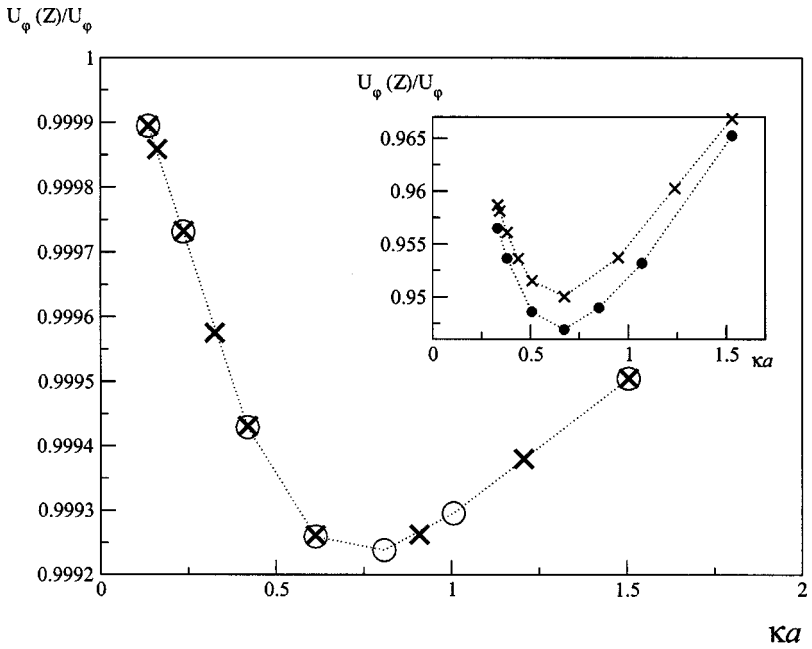

FIG. 5. Reduced sedimentation velocity of a periodic array of colloids of valency $Z=10$ in an electrolyte as a function of κa. The figure shows the results for two different values of the ionic diffusion coefficients. The curve for $D_0^{(1)}=0.95$ (circles) has been rescaled to the curve for $D_0=0.19$ ($\times$) according to Eq. (37), i.e., $U(D)=U(D_0^{(1)})*(D_0^{(1)}/D_0)$. The superposition of the two curves shows that the scaling is obeyed. In the inset we also show the results for a colloid of valency $Z=100$. However, in this high-charge regime the sedimentation velocity does not scale with the diffusion coefficient in the way predicted by the linearized theory.

is a small variation in the numerical value of the sedimentation velocity. However, this difference already shows up for sedimentation of a neutral sphere. It is due to a small change in the fluid viscosity that is caused by a small difference in the overall fluid density in the two implementations. The valency of the macro-ion was chosen to be $Z=10$, which corresponds to the small charge limit. Although our computational scheme should also work outside the Debye–Hückel limit, we restrict ourselves to this regime, because it is only in this limit that we can compare with existing analytical results. Specifically, Booth predicted that the sedimentation velocity, $U_0(Z)$, of a weakly charged sphere of valency Z in the dilute limit can be expressed as[18]

$$\frac{U_0(Z)}{U_0}=1-c_2Z^2, \tag{36}$$

where U_0 is the sedimentation velocity of a neutral sphere, and c_2 is a constant that can be computed analytically in the Debye Hückel limit. For the simplified situation of monovalent co- and counterions, $z_+=-z_-=1$, which have the same diffusivity, $D_+=D_-=D$, the expression for c_2 simplifies to

$$c_2=\frac{k_BTl_B}{72\pi a^2\eta D}f(\kappa a), \tag{37}$$

where $f(\kappa a)$ is a linear combination of exponential integral functions[7] and is a function of the inverse Debye length, $\kappa=\lambda_D^{-1}=\sqrt{4\pi l_B\Sigma_k z_k^2\rho_k}$. We have checked that the sedimentation velocity scales as predicted with the viscosity. We have also verified that we are indeed in the linear regime where the sedimentation velocity is proportional to the applied gravitational field. In particular, for the two values of the density considered, ρ_s, the linear regime was obtained for forces per unit of volume such that the flow velocity never exceeded 0.1 in lattice units.

Figure 5 shows the sedimentation velocity of a weakly charged sphere ($Z=10$) as a function of the inverse Debye screening length. As can be seen from the figure, the sedimentation velocities scales with the ionic diffusivity in the way predicted by Eq. (37). The inset in the same figure shows that this scaling breaks down at higher colloidal charges ($Z=100$), i.e., outside the range of validity of the linearized Poisson–Boltzmann description.

Figure 6 shows the reduced sedimentation velocity $[U_\varphi(Z)/U_\varphi(Z=0)]$ as a function of κa for a range of volume fractions. As the volume fraction decreases, the curves approach Booth's infinite-dilution result, while the minimum sedimentation velocity moves toward the minimum value predicted by theory. In order to compare quantitatively the simulation results with Booth's theory, Eq. (36), we must extrapolate the computed values for $U_\varphi(Z)/U_\varphi(Z=0)$ from the finite φ values of the simulations to the infinite-dilution limit, $U_0(Z)/U_0(Z=0)$. For neutral spheres Hashimoto has shown that that the sedimentation velocity converges very slowly to its infinite-dilution value, namely, as[20]

$$\frac{U_\varphi(Z=0)}{U_0(Z=0)}=1-1.7601\varphi^{1/3}+\varphi+O(\varphi^2), \tag{38}$$

Ladd has numerically verified this dependence.[21] For charged spheres, due to the electrostatic screening, we still expect that the dominant φ dependence comes from excluded volume; previous results indicate that this is indeed the case[7]. When performing the dilute limit expansion, we therefore decided to single out the major volume fraction dependence by normalizing the simulation results with the Stokes drag coefficient, i.e., computing the low-density limit of $U_\varphi(Z)/U_0(0)$. As a result, it is reasonable to obtain the same functional dependence on φ as Hashimoto with a slightly different amplitude. Specifically, we expect

$$\frac{U_\varphi(Z)}{U_0(0)}=1-(1.7601+\epsilon)\varphi^{1/3}+O(\varphi^{2/3}), \tag{39}$$

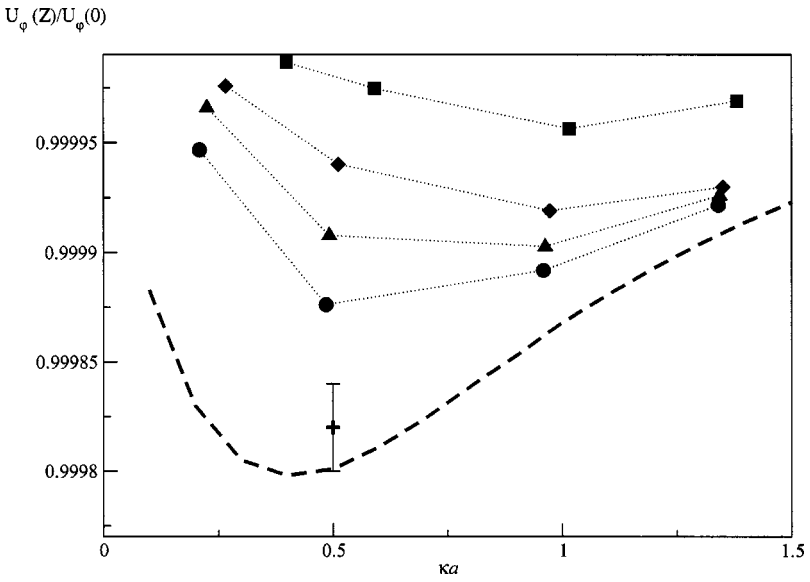

FIG. 6. Sedimentation velocity of a periodic array of spheres of valency $Z=10$ and hydrodynamic radius $a=4.3$. The Bjerrum length $l_B=0.4$ (in lattice units). The diffusion coefficient of both positive and negative ions is set to $D=0.19$. We compare simulation results for finite volume fractions, namely 0.0416 (squares), 0.0123 (diamonds), 0.005 21 (triangles), and 0.002 67 (circles) against the Booth theory, which is valid at infinite dilution (dashed curve). For $\kappa a=0.5$ we also show the estimated value of the sedimentation velocity at infinite dilution (see the text). The point corresponds to the extrapolation of the law, Eq. (39). Within the estimated error, the extrapolated simulation results agree with the predictions of Ref. 18.

where ϵ is much less than one. Eventually, the dilute limit is obtained by extrapolating Eq. (39) to $\varphi=0$.

In Fig. 6 we show the extrapolated sedimentation velocities for a particular value of κa. The estimated error in the limiting sedimentation velocity is rather large. It could have been reduced by computing more values of the sedimentation velocity at low volume fractions. In addition, there is some uncertainty in the value of the effective sphere radius. In light of these uncertainties, the agreement with the Booth limit in Fig. 6 is gratifying.

D. Absence of spurious fluxes

We pointed out in Sec. III that one of the incentives for developing the present model was to eliminate any mixing of continuous-space gradients and discretized gradient operators. The reason is that the inevitable approximations associated with the discretization of gradient operators usually lead to the appearance of spurious mass and momentum fluxes, even in equilibrium. Such spurious fluxes are present, in particular, whenever there exist spatial inhomogeneities related, for example, to the presence of liquid interfaces. In the present approach, we only use lattice-gradient operators that have been constructed such that, in equilibrium, no flow can result. To demonstrate the effect that this has, we compare the present method with an existing ''mixed'' method. In particular, we consider a spherical colloid of radius $a=4.5$, at rest in an electrolyte in a cubic box of diameter $L=20$. The valency of the sphere is $Z=10$ and the system as a whole is electrically neutral. In Fig. 7 we show the projection of the momentum flux in the equatorial plane of the sphere and compare these residual fluxes both for the model introduced in this paper and the model of Ref. 7. Figure 7(a) shows that spurious currents, although small, are certainly not negligible in this case. Moreover, their magnitude is clearly correlated with the distance to the colloidal particle: the largest currents appear in the region where the spatial gradients are largest. For highly charged spheres (i.e., outside the linear Debye–Hückel regime) these spurious fluxes will become larger. In contrast, in Fig. 7(b) (the present model), the spurious fluxes are at the level of machine precision. In fact, to make them visible at all, we had to multiply the momentum fluxes by a factor 10^{13} relative to the old model. In other words, the residual fluxes are controlled by machine accuracy. Even at this level one cannot detect a correlation between the fluxes and the position of the sphere. We can conclude that the proposed model eliminates the appearance of spurious equilibrium fluxes.

VII. CONCLUSIONS AND DISCUSSION

We have introduced a new model to simulate the collective dynamics of nonideal fluid mixtures, with a special emphasis on its use to study electrokinetic phenomena. The method relies on a lattice-Boltzmann model, where the interactions are introduced as effective forces. In this respect, our model resembles a Vlasov kinetic model, as opposed to previous kinetic lattice models. In our approach the fluxes between neighboring lattice nodes are the fundamental dynamical objects that couple external fields to both electrical conduction and hydrodynamic flow.

As a result of the symmetric formulation of the flux between neighboring nodes we can impose strict local mass conservation. As a consequence, the present model is free of spurious boundary fluxes that plague all other lattice-Boltzmann models of fluid mixtures. Moreover, a link-based description has the additional advantage that boundary conditions are easily implemented.

Second, by using a multistep approach, we can vary ionic mobilities over many orders of magnitude. This feature of our model allows us to explore electroviscous effects over a wide range of Peclet numbers. We have shown that flow causes spurious advection diffusion. However, this effect is well understood and can be made negligible in most practical cases.

We have checked the performance of the model by studying equilibrium diffuse layers, showing that it is possible to recover both low- and high-charge density regimes. In the latter, the only limitation is related to computational resources, because a finer grid is required to resolve the nar-

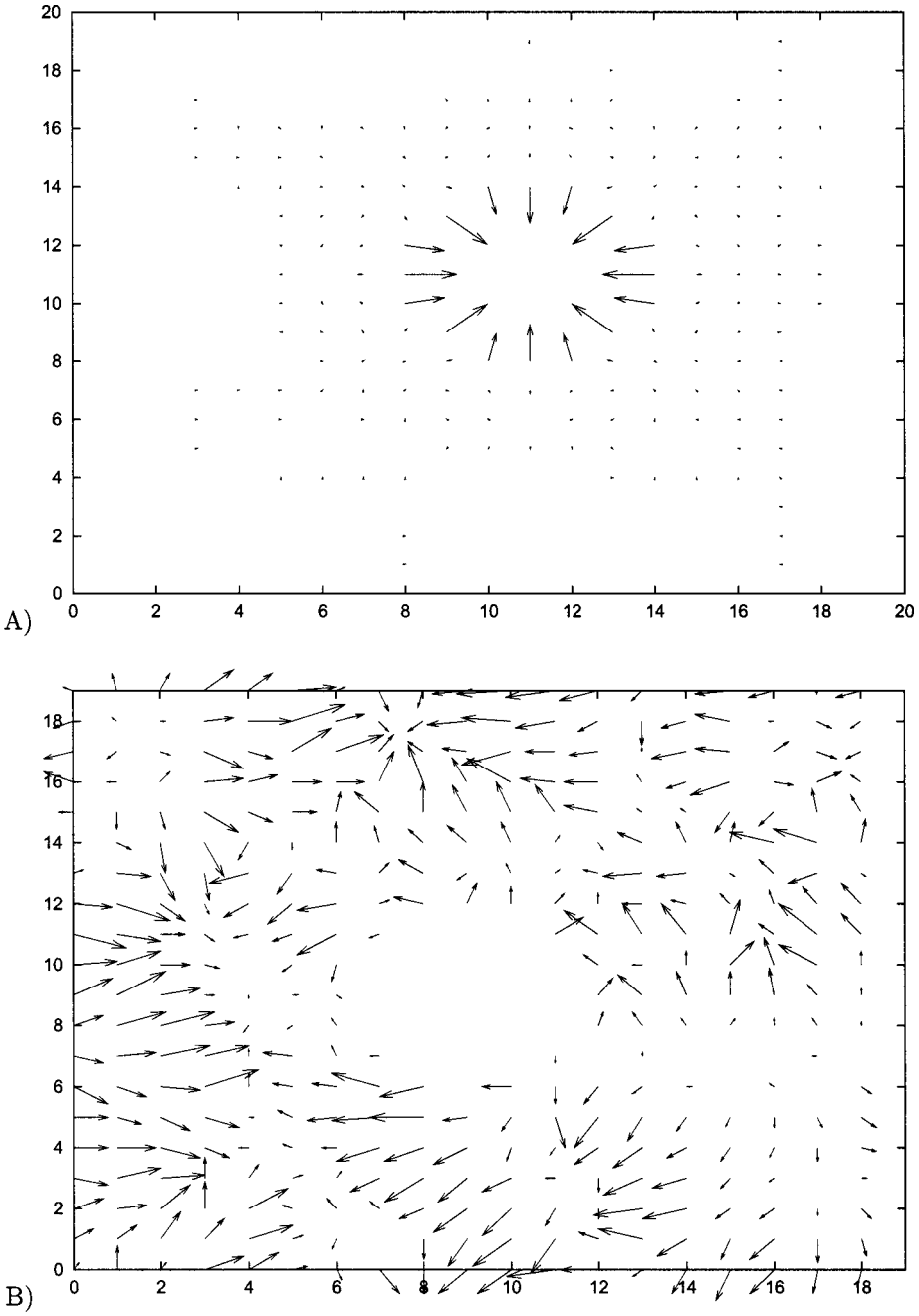

FIG. 7. An illustration of suppression of spurious boundary currents in the present LB model. In the figure we compare the apparent currents in equilibrium for two models: figure (a) gives the results for the model described in Ref. 7; (b) shows the results for the present model. In both cases we consider a colloidal sphere of radius 2.5 in a system with a diameter $L=20$ lattice spacings. As there are no external forces acting on the system and the colloid is not moving, the fluid is supposed to be at rest. The figure shows the measured projection of the momentum flux in the equatorial plane of the colloid. In (a), spurious currents are apparent close to the particle surface. The spurious currents in case (b) are much smaller than in case (a). In fact, to make them visible at all, they have been scaled up by a factor 10^{13} with respect to case (a). This is an indication that the spurious currents in case (b) have been suppressed down to machine accuracy.

rower charge profiles that develop nearly highly charged walls. To test the coupling of electrostatics and fluid flow, we have computed the sedimentation velocity of a charged sphere. These simulations indicate that the existing theoretical predictions are reproduced in the low-charge, low-density limit. As the charge of the colloid is increased, the simulation results start to deviate from the theoretical predictions that apply in the linearized Poisson–Boltzmann regime.

Even though in the present paper we have focused on electrostatic interactions and, in particular, we have not discussed molecular interactions that favor demixing, such interactions could also be incorporated in the present model.

ACKNOWLEDGMENTS

The authors thank C. P. Lowe for very useful discussions. This work is part of the research program of the ''Stichting voor Fundamenteel Onderzoek der Materie (FOM),'' which is financially supported by the ''Nederlandse organisatie voor Wetenschappelijk Onderzoek (NWO).'' I.P. acknowledges partial financial support from DGICYT of the Spanish Government, and thanks the FOM Institute for its hospitality.

[1] *Electrostatic Effects in Soft Matter and Biophysics*, NATO Sci. Series, edited by C. Holm, P. Kèkicheff, and R. Podgornik (Kluwer Academic, Dordrecht, 2001).
[2] W. M. Gelbart, R. F. Bruinsma, and P. A. Pincus, Phys. Today **53**, 38 (2000).
[3] R. F. Probstein, *Physicochemical Hydrodynamics* (Butterworths, Boston, 1989).
[4] A. D. Stroock, S. K. W. Deringer, A. Ajdari, I. Mezic, H. A. Stone, and G. M. Whitesides, Science **295**, 647 (2002).
[5] R. D. Groot, J. Chem. Phys. **118**, 11265 (2003).
[6] P. B. Warren, Int. J. Mod. Phys. C **8**, 889 (1997).

[7] J. Horbach and D. Frenkel, Phys. Rev. E **64**, 061507 (2001).
[8] W. R. Osborn, E. Orlandini, M. R. Swift, and J. M. Yeomans, Phys. Rev. Lett. **75**, 4031 (1995); M. R. Swift, E. Orlandini, W. R. Osborn, and J. M. Yeomans, Phys. Rev. E **54**, 5041 (1996).
[9] S. R. de Groot and P. Mazur, *Non-Equilibrium Thermodynamics* (Dover, New York, 1984).
[10] S. Succi, *The Lattice Boltzmann Equation for Fluid Dynamics and Beyond* (Oxford University Press, Oxford, 2001); R. Benzi, S. Succi, and M. Vergassola, Phys. Rep. **222**, 145 (1992).
[11] A. J. C. Ladd and R. Verberg, J. Stat. Phys. **104**, 1191 (2001).
[12] Z. Guo, C. Zheng, and B. Shi, Phys. Rev. E **65**, 046308 (2002).
[13] L.-S. Luo and S. S. Girimaji, Phys. Rev. E **66**, 035301 (2002).
[14] A. J. C. Ladd, J. Fluid Mech. **271**, 285 (1994).
[15] N.-Q. Nguyen and A. J. C. Ladd, Phys. Rev. E **66**, 046708 (2002).
[16] W. H. Press, S. A. Teukolski, and W. T. Vetterling, *Numerical Recipes* (Cambridge University Press, Cambridge, 1996).
[17] J. N. Israelachvili, *Intermolecular and Surface Forces* (Academic, New York, 1991).
[18] F. Booth, J. Chem. Phys. **22**, 1956 (1954).
[19] A. J. C. Ladd, J. Fluid Mech. **271**, 311 (1994).
[20] H. Hashimoto, J. Fluid Mech. **5**, 317 (1959).
[21] A. J. C. Ladd, J. Chem. Phys. **93**, 3484 (1990).